AIAA JOURNAL
Vol. 48, No. 5, May 2010

Numerical Study of Acoustic Installation Effects with a Computational Aeroacoustics Method

S. Redonnet,* G. Desquesnes,† and E. Manoha‡
ONERA, Châtillon 92322, France
and
C. Parzani§
Airbus Industries, BP M01 32/7, F-31060 Toulouse Cedex 03, France

DOI: 10.2514/1.42153

This paper deals with the numerical study of installation effects, a subject which comes under the more general purpose of aircraft noise prediction and reduction. As an example of installation effects, we study here the potential acoustic shield that an empennage airfoil could constitute against the aft fan noise emitted by a coaxial engine. To that end, we make use of a structured computational aeroacoustics solver (*sAbrinA* code), taking benefits from its coupling functionality in order to handle more easily the solid obstacles that are to be accounted for. Several full-3D simulations are then conducted, which involve an exhaust installed over an empennage airfoil and allotted with two thermodynamics conditions (quiescent medium and takeoff flight). Being validated against boundary element method results, such calculations provide a validation of the numerical strategy adopted here as well as a good illustration of its abilities to solve installed engine noise problems. Coming in addition to such methodological outcomes, these calculations deliver important conceptual insights, demonstrating the potential high efficiency of empennage airfoils in terms of aft fan noise reduction.

Nomenclature

kR	=	reduced frequency (with respect to the outer radius of the engine's secondary exhaust)
λ, λ^*	=	wavelength and apparent minimum wavelength, respectively
M^∞	=	steady mean-flow Mach number (at infinity)
PPW*	=	(grid) points per apparent wavelength
p_o, p_o^∞	=	steady mean-flow pressure (local and at infinity, respectively)
q_o, q_o^∞	=	steady mean-flow kinetic energy (local and at infinity, respectively)
R	=	outer radius of the engine's secondary exhaust
T	=	acoustical source period
U_o^{exhaust}	=	steady mean-field flow, in the exhaust vicinity
U_o^{airfoil}	=	steady mean-flow field, in the airfoil vicinity
U_o^∞	=	steady mean-flow field, at infinity
v_o, v_o^∞	=	steady mean-flow velocity (local and at infinity, respectively)

I. Introduction

WITHIN several French national programs and European projects, Airbus is leading studies of new aircraft concepts driven by installation effects, which are interesting aircraft designers more and more. Among the most promising concepts, the rear fuselage nacelle (RFN) [1,2] configuration, based on mounting the engines at the rear fuselage above the empennage (see Fig. 1), takes advantage of a nonnegligible acoustical shielding effect by the airframe on aft fan noise emissions.

The acoustic installation effects characterizing such a RFN configuration were recently investigated, with the help of ONERA's full Euler's equation (FEE) solver named *sAbrinA*. Taking benefits from a coupling methodology recently developed in it, such structured computational aeroacoustics (CAA) solver was used to numerically assess the aft fan noise propagation/radiation of a 3D exhaust, the latter being 1) installed over an empennage airfoil, 2) affected by realistic thermodynamic conditions (takeoff flight), and 3) allotted with a representative fan noise modal content.

The present article aims at summarizing the main outcomes that such a numerical study delivered, from both a methodological and a conceptual point of view. To that end, this paper will first introduce the configuration that was numerically investigated, replacing it within its context. Then, other works conducted on related matters by various authors will be reviewed, the relevance of the numerical strategy adopted here being then underlined. The main features of the latter will then be summed up, a special emphasis being put on its coupling methodology. Then, results of several 3D numerical simulations will be displayed, providing a validation of the present methodology as well as a good illustration of the potential gain that RFN configurations could offer regarding aft fan noise reduction concerns.

II. From the Simulation of Aft Fan Noise of Isolated Coaxial Engines Toward a Prediction of RFN Installation Effects

Fan noise is a major harmful aircraft sound source, especially during takeoff or approach flight phases. For a long time, engine and aircraft manufacturers only investigated the prediction/reduction of the fan noise upstream component, which is emitted by the engine's air intake. For a few years, they have also been investigating the more complex problem of predicting/reducing its downstream component, which is radiated through the exhaust and its heterogeneous jet flow.

In previous studies [3–5], ONERA's computational fluid dynamics (CFD)/CAA calculation platform named *sAbrinA* [6–9] was used to simulate the aft fan noise propagation of several (2D or 3D-axi) coaxial engines, the latter being considered under an isolated

Presented as Paper 3501 at the 13th AIAA/CEAS Aeroacoustics Conference (28th AIAA Aeroacoustics Conference), Rome, 21–23 May 2007; received 12 November 2008; revision received 31 May 2009; accepted for publication 20 September 2009.

*PhD, Research Scientist, CFD and Aeroacoustics Department, ONERA–BP 72, 29 av Division Leclerc, F-92322.
†PhD, Research Scientist, CFD and Aeroacoustics Department, ONERA–BP 72, 29 av Division Leclerc, F-92322.
‡PhD, Research Scientist, CFD and Aeroacoustics Department, ONERA–BP 72, 29 av Division Leclerc, F-92322.
§PhD, Engineer, Department of Acoustic and Environment, Airbus SAS, BP M01 32/7, F-31060.

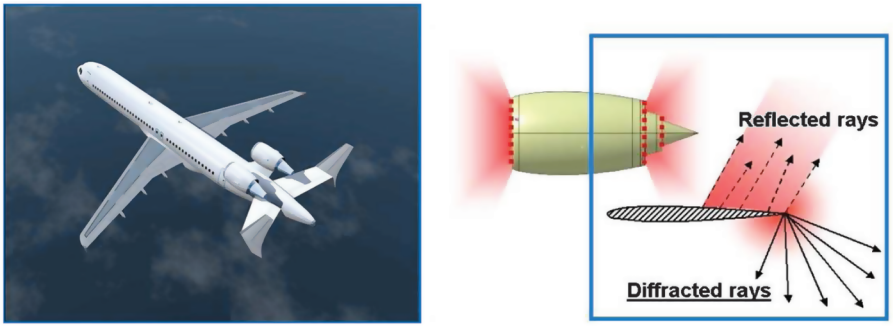

Fig. 1 Artist (left) and schematic (right) views of the RFN concept (courtesy of Airbus France).

configuration (i.e., without any airframe integration). In particular, these computations correctly accounted for the refraction effects due to the (strong) heterogeneities of the jet mean flow [4,5]. Here, it has to be said that such a challenge could only be achieved by the use of a CAA code such as *sAbrinA*. As a reminder, one can comment that this (structured) solver is based on a conventional hybrid process in which a preliminary aerodynamic calculation provides a heterogeneous steady mean flow, on which an acoustic calculation can then be performed, before being possibly postprocessed using another method (Kirchhoff or Boundary Element) that provides the far-field radiation.

Once this ability to correctly simulate the aft fan noise propagation of an isolated engine was confirmed, it was decided to take a further step toward the prediction of installed (or aircraft integrated) coaxial engines, through the numerical assessment of acoustic shielding effects potentially offered by a RFN configuration onto aft fan noise emissions. More precisely, the task consisted in simulating the 3D aft fan noise propagation/radiation characterizing a coaxial engine, the latter being 1) installed over an empennage airfoil, 2) considered within takeoff thermodynamic conditions (with a highly heterogeneous jet mean flow), and 3) allotted with pertinent aft fan noise contents (in terms of frequency and mode azimuthal/radial orders).

On this stage, one needs to underline the relevance of such a full-CAA approach, with respect to other numerical strategies previously adopted by various authors regarding similar concerns. As extensively shown by Dunn and Tinetti [10–12], methods solving the Helmholtz equation in the presence of solid boundaries [boundary element method (BEM), fast multipole method, etc.] are particularly well-suited to address such installed engine noise problems, in which aircraft devices present realistic (and thus complicated) geometries. However, despite the real advantages such methods effectively offer in terms of reduced meshing and computing efforts, they cannot account for all the refraction effects resulting from the (most severe) mean-flow gradients, which is absolutely required when considering exhaust noise problems [2,4,5,13,14] such as the present one, in which acoustic waves have to cross the highly heterogeneous jet mean flow. As shown by Redonnet et al., this intrinsic limitation of BEM solvers can always be relaxed through a proper coupling with a CAA tool, this resulting in a hybrid CAA/BEM approach [2]. However, although such a hybrid method effectively offers an excellent compromise in terms of an accuracy-vs-flexibility ratio, it is more easily useable in a CAA $\rightarrow$ BEM weak-coupling sense, which implies that all secondary acoustic reflections occurring between solid obstacles are to be neglected.

From what precedes, it turns out that only a full-CAA methodology seems able to ensure the best level of accuracy, with respect to both refraction and reflection phenomena underlying realistic installed engine noise problems. Here, we must remember that Stanescu et al. [15,16] pioneered on this topic by assessing through a full-CAA unstructured method [discontinuous Galerkin method (DGM)] the acoustic installation effects induced onto the forward fan noise by a wing and/or part of a fuselage. Although it was there applied only to an engine inlet without any background mean flow, such a DGM approach can handle more severe configurations such as the one addressed here. Considering that, compared with their unstructured counterparts, full-CAA structured methods generally require lighter CPU resources, it appears that the latter are capable of answering such installed engine noise questions at least as efficiently as the former. This fact (assessment of which constituted an indirect objective for the present study) nevertheless implies that the intrinsic meshing constraints which structured CAA methods are submitted to can be relaxed in a proper way, such as the one presented below.

Indeed, the present calculations (or, more precisely, their preliminary meshing tasks) were greatly lightened thanks to a coupling technique that had been previously developed at ONERA [17,18]. With such a technique (details of which are given below), it becomes possible to mesh several solid bodies in a completely independent way, the single common point between all different grids being the usual minimum points-per-wavelength criteria. These independent body-fitted curvilinear grids can then be sunk within a wider Cartesian background mesh, the role of which will be to make them communicate by transmitting the instantaneous perturbations from one to the other at each time step. Such a coupling methodology/functionality has already been validated in its 2D version, through both academic and industrial 2D test cases (such as the acoustic diffraction over two cylinders [18] or over a high-lift wing [17]). In addition, a simplified 2D version of the present installed exhaust problem has allowed us to further 2D-validate such a coupling feature, as well as to preliminarily assess how the latter could help in CAA-handling such installed engine noise configurations [19]. The present study was the step required for extending these preliminary works of methodological validation and conceptual assessment in a more realistic sense.

III. The CAA Methodology and Solver

A. Numerical Method and Features

The *sAbrinA* solver is a multipurpose integrated CFD/CAA platform that was developed at ONERA [6–9]. This structured code can solve both the Euler and Navier–Stokes equations, the latter being taken under a conservative and possibly perturbed formulation (with a splitting of the complete variables into a frozen mean-flow quantity and a fluctuating perturbed one). The solver deals with multidimensional/multiblock structured grids, as well as several boundary conditions (solid wall, symmetry, outflow, etc.). It also offers a wide set of time and space schemes (finite differences and finite volumes, of low or high order, etc.).

As regards CAA purposes in particular, *sAbrinA* solves the FEE in perturbation, with the help of high-order finite differences spatial (6th order) and filter (10th order) schemes, combined with a (three-level) Runge–Kutta time scheme. Relative to the surrounding free-field boundaries, a conventional characteristic method [20,21] is coupled with a grid stretching (over eight rows of ghost points), in order to let the perturbations leave the calculation domain correctly, that is to say without generating noticeable numerical reflections at the frontiers.

For detailed information about the *sAbrinA* solver and its underlying methodology, we refer the reader to the references [6–9], where both are fully described.

B. Coupling Methodology/Functionality

Several overlapping (or overset) methods especially dedicated to CAA have recently been proposed in the literature [22–24]. One must

remember that all these methods are a high(er)-order extension of classic Chimera approaches developed for CFD purposes. In the same way, the present coupling method is based on a CFD Chimera method initially developed by Steger et al. [25]. Such a coupling technique having been described and analyzed in detail in [17,18], only its main characteristics will now be reviewed.

Let us consider a body-fitted curvilinear grid overlapped by a Cartesian mesh, as sketched on the left side of Fig. 2. Two coupling areas (here, in red and green) can be defined so that a double data transfer (from one grid to the other, and vice-versa) is performed at each step of the temporal integration process. More precisely, each one of the two coupling areas will be dedicated to a particular sense in the data transfer (curvilinear $\rightarrow$ Cartesian in red, or Cartesian $\rightarrow$ curvilinear in green), the latter consisting in an interpolation process.

Such a double data transfer process aims at ensuring the best level of efficiency and safety to the coupling technique. Indeed, both coupling areas being narrow, the amount of data transfer (and thus interpolation operations) that are to be achieved between all grids is here minimized at maximum, which obviously decreases the CPU time to be spent in data exchanges. Apart from that, each one of the coupling zones being dedicated to a particular sense of data transfer, the risk of cross-corrupting the perturbations to be solved on each grid is here avoided. In particular, no interpolating point can be erroneously interpolated, from the moment that both coupling areas are separated by a minimal distance (given by the half-width of the space scheme's stencils). In addition, all unphysical quantities that might be generated in certain regions will remained confined there. As an example, considering the Cartesian grid, it can be noticed that the near-field region included within the curvilinear $\rightarrow$ Cartesian interpolation area (in gray, Fig. 2) has no physical sense. But, thanks to the explicit forcing provided by the curvilinear $\rightarrow$ Cartesian data transfer, these unphysical perturbations will remain confined within this near-field region, being then unable to pollute the mid/far-field ones. In the same way, considering this time the body-fitted curvilinear grid, it can be seen that all the spurious waves that could ever be generated by its peripheral boundaries will remain confined far from the obstacle, their propagation being cancelled by the Cartesian $\rightarrow$ curvilinear retroaction (green area).

Concerning the high-order interpolation process itself, let us recall that Lagrange polynomials offer the best quality–price ratio, since they present both a good accuracy and a light CPU-time consumption. In particular, all the results presented in this study were obtained with the help of a coupling functionality involving Lagrange polynomials of 6th order. Here, it is also worth underlining the fact that, if the Cartesian $\rightarrow$ curvilinear interpolation coefficients can be easily obtained, the identification of the curvilinear $\rightarrow$ Cartesian interpolation coefficients is not straightforward at all. A way to solve this problem is to stick up the curvilinear system of coordinates into an intermediate Cartesian one (referred to as the reference domain; see the right-hand side of Fig. 2). This is made with the help of polynomial approximations, each one being evaluated through the numerical inversion of a linear system [17]. Finally, one can comment that the calculation of the Cartesian $\rightarrow$ curvilinear and curvilinear $\rightarrow$ Cartesian interpolation sets to be applied is conducted only at the initialization stage of the CAA simulation, once the grids have been loaded.

IV. Numerical Characterization of RFN's Acoustic Installation Effects, Through the Application and Subsequent Validation of the Coupling Methodology

A. Test Case Description

Let us consider a coaxial engine of realistic shapes and dimensions (in the following, R indicates the outer radius of the secondary exhaust), such engine being located over an empennage airfoil. We propose numerically highlighting how the latter could constitute an efficient acoustic shield for the engine's aft fan noise emissions.

For the sake of simplicity, as fan noise to be emitted upstream of the secondary exhaust, we will consider the sole spinning mode (2, 2), of reduced frequency $kR = 11.84$. Here, one can comment that such acoustic input was prescribed since it is quite representative of a real engine aft fan noise component. In particular, for an engine at its full thrust (or under takeoff conditions, as considered here), such a modal frequency corresponds to one half of the blade passing frequency. On that stage, one can also comment that the exhaust $\leftrightarrow$ airfoil relative positioning was chosen with regard to specific industrial constraints and expectations (in terms of potential acoustic shielding).

B. Grids Generation

According to what was previously said concerning the coupling method, three CAA grids were built for this two-obstacles problem.

Two body-fitted curvilinear meshes (surrounding, respectively, the nozzle and the airfoil) were first derived from CFD grids initially constructed and used for the associated (Reynolds-averaged Navier–Stokes (RANS) mean-flow calculations (see Sec. IV.E). Such a CFD $\rightarrow$ CAA grid derivation was conducted with the *ReMesh2D* tool [4,5], an ONERA in-house code that makes it possible to 1) entirely remesh any 2D (structured multiblocks) CFD grid into a CAA one, 2) interpolate on the latter the CFD background mean flow, and 3) possibly extend all this grid and flow material in a third dimension. In the present case, such a remeshing task led to two 3D meshes of, respectively, five domains (206,258 nodes, for the nozzle) and two domains (989,055 nodes, for the airfoil) of a $4R$ wingspan extent (see Fig. 3).

Here, one can comment that these girds were constructed with a concern for sufficient resolution in terms of points per (apparent minimum) wavelength (PPW*). Such a quantity can be estimated as $\lambda^* = \lambda(1 - M^\infty)$, where λ stands for the wavelength and M^∞ represents the infinite Mach number ($M^\infty = 0.25$ in the present case). This PPW* criterion was here set to a minimum value of 15, guaranteeing a good resolution of acoustic waves in both the upstream and the downstream directions. Let us emphasize that with such a criterion, the engine's secondary exhaust was sufficiently discretized (with 11 points in the radial direction) to properly capture the radial profile of the emitted fan noise mode (of radial order 2).

A third mesh was then constructed under the same PPW* constraint, providing a background Cartesian monodomain grid of 9,049,830 nodes. As said previously (Sec. III.A), to enhance the exit of perturbations out of the calculation domain, a stretching was applied to the eight peripheral rows of points of this background mesh, the last row being allotted with a characteristic [20,21] boundary condition.

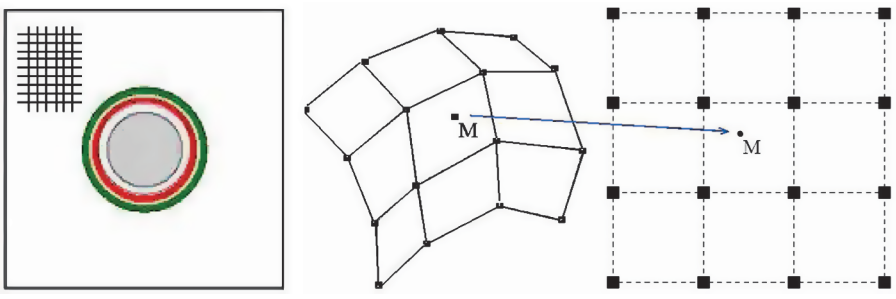

Fig. 2 The coupling method principle.

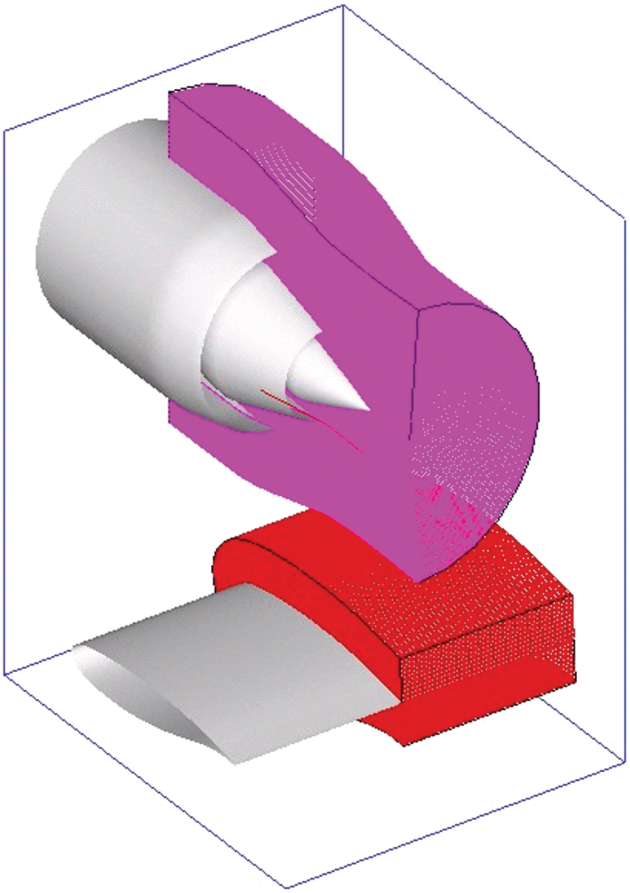

Fig. 3 The two body-fitted grids.

Figure 3 provides a view of the two curvilinear body-fitted grids, encompassing, respectively, the exhaust (in purple) and the airfoil (in red). On the same figure are plotted the limits of the background Cartesian domain (in blue), which defines a useful computational box of approximately $5R \times 4R \times 4R$.

Concerning the application of the coupling process to the present problem, Fig. 4 sketches the double data transfer to be applied between the background Cartesian mesh and each one of the two curvilinear grids. Here, we can remember that such a double data transfer implied only four distinct sets of interpolation points (see Sec. III.B), the two first sets being devoted to the exhaust $\Leftrightarrow$ background grids communication, while the two last ones were dedicated to the background $\Leftrightarrow$ airfoil meshes one.

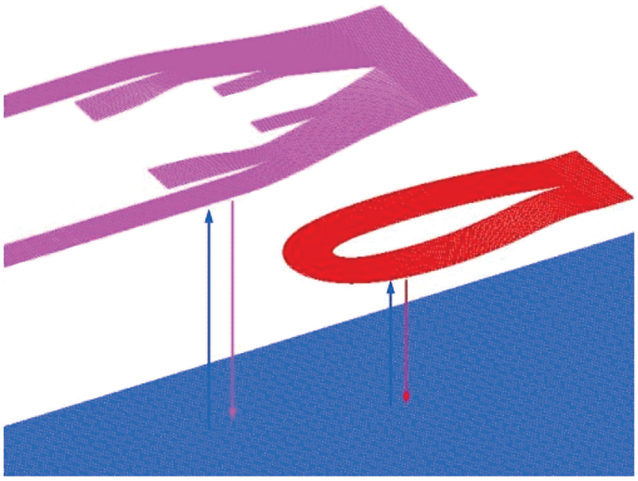

Fig. 4 The coupling principle.

C. Aft Fan Noise Radiation of the Installed Engine Taken Under a No-Flight Condition (Quiescent Medium)

Since the present problem constituted a first attempt for applying the coupling methodology/functionality to a 3D industrial-like case, it was decided to perform it first with a no-flight condition (i.e., over a medium at rest).

The time step was set to a value corresponding to one 140th of the aft fan noise source period T, providing an acceptable Courant–Friedrichs–Lewy (CFL) number (0.9). Once the four distinct sets of curvilinear points to be interpolated were (automatically) detected and their respective interpolation coefficients were computed, the calculation was started. It was run until the stationary state was established over the computational domain, which required 14,351 sec (4 h CPU) on the ONERA NEC-SX8 super computer. Regarding the number of grid points (10,245,143 cells) and iterations (2100 steps) this calculation involved, such a CPU time indicates an average computational time of 0.667 μ sec/iteration/cell, a value that matches usual *sAbrinA* performances; from such an observation, it can thus be stated that the coupling process does not really weigh on the overall computational time, which is obviously due to the fact that the interpolation points represent only a small fraction of the total grid points (see Sec. IV.B).

Figure 5 displays two plots of the instantaneous perturbed pressure field obtained at the end of the simulation.

From a purely numerical point of view, one can first notice the perfect continuity of acoustic wave fronts over the entire domain, and more particularly at the curvilinear/Cartesian grids interfaces (slight discrepancies of Fig. 5's right side being purely graphical). Considering the quite complicated character of such a configuration involving two full-3D obstacles, one can thus be convinced of the coupling technique accuracy. Secondly, one can also note the efficiency of the free-field condition imposed on the peripheral rows of the Cartesian domain, which do not seem to generate any noticeable reflection (see for instance the upper and front sides of the half-domain Cartesian box, on the left side of Fig. 5).

From a more physical point of view, a brief overview of their acoustical patterns indicates that, as they propagate outside the secondary exhaust, the acoustic waves are submitted to successive reflections from the two obstacles. A set of interferences then establishes itself between both the lower part of the engine and the upper part of the airfoil (suction side). By observing now what occurs in the very lower part of the calculation domain (under the profile), it appears immediately that the airfoil acts as an efficient shield against the sound emitted toward the ground. Only a fraction of it succeeds in diffracting and escaping outside the profile. At this stage, it has nevertheless to be emphasized that such a result is strongly driven by the particular directivity pattern (and thus modal content) of the aft fan noise considered here, as well as by the present airfoil shielding/reflecting characteristics (i.e., dimensions/relative location to the engine). Any other set of acoustical/structural characteristics should obviously lead to different observations (at least in a quantitative way), resulting in another acoustic shielding effect.

D. Validation Against a Boundary Element Method Computation

To validate these results (and, more particularly, the methodology used to obtain them), the previous computation was conducted again, but this time with the help of a BEM. As a reminder, BEM codes (harmonically) solve the Helmholtz equation for a given set of (solid) boundary conditions, allowing to predict all the reflection/diffraction effects due to the interactions occurring between a monochromatic acoustic source and any solid obstacle(s), all that being achieved under a homogeneous medium hypothesis.

A three-dimensional BEM model of the present nozzle + airfoil configuration was built with the help of 65,919 nodes/131,830 (surfacic) elements. Then, the acoustic excitation [mode (2, 2), $kR = 11.84$] having been imposed upstream of the secondary nozzle,

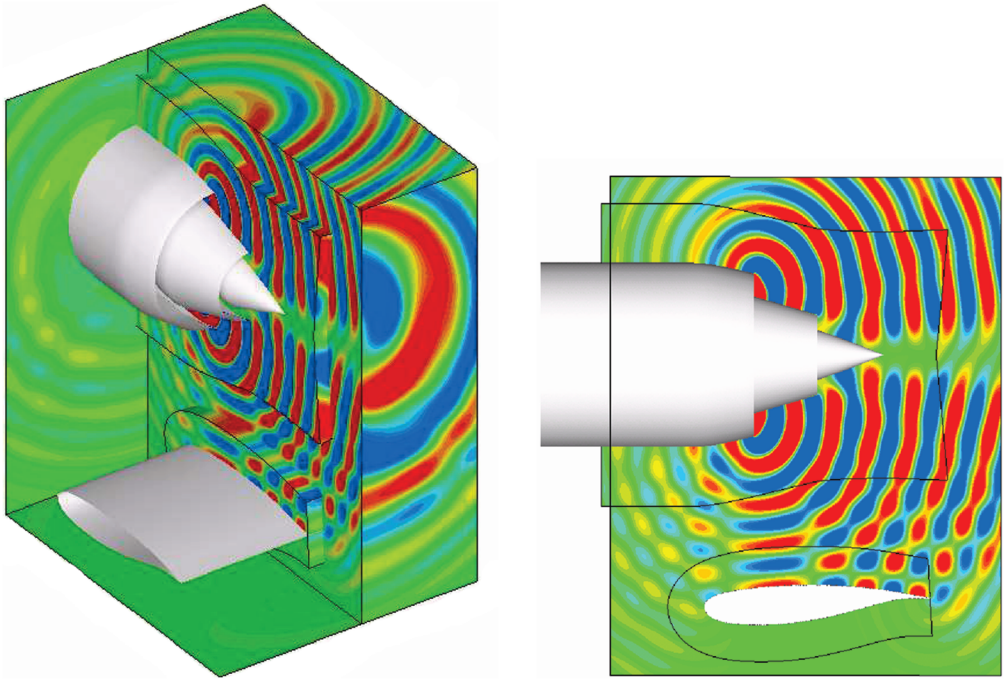

Fig. 5 Aft fan noise radiation of the installed engine in no-flight conditions (quiescent medium). sAbrinA calculation: instantaneous perturbed pressure field obtained at the end of the simulation, plotted over both a 3D domain (of half the computational domain, left side) and a lateral plane (right side).

the pressure field was computed within two bidimensional planes crossing the domain. Such calculation was conducted by the Airbus-France Acoustic and Environment Department, with the help of the BEM code named *ACTI3S* [26], a solver initially developed by European Aeronautic Defense and Space Company's Common Research Center.

Figure 6 compares both the perturbed pressure field computed using *sAbrinA* (at the beginning of a source cycle) and the real part of the BEM complex pressure computed using *ACTI3S*. As it can be seen, both results agree very favorably, even over regions where acoustic patterns present very low amplitudes.

Another comparison is provided in the upper part of Fig. 7, where the same results are plotted along two cuts (displayed in red, on the left lower part of the same figure). Again, a very good agreement is observed between the results, although some slight discrepancies remain. Since it has been checked that they were not induced by an insufficient convergence of the CAA solution, such differences could be explained by the fact that, due to methodological/computational (CPU) constraints, the choice was made of BEM computing the totality of the wingspan extent, while the *sAbrinA* calculation was only calculated over a well-resolved maximum wingspan extent of $4R$ (in black on Fig. 7's right lower quarter), the airfoil extra extension (in red) being sunk within the stretched zone and, thus, poorly solved. It is obvious that under these conditions, the respective *ACTIS3S/sAbrinA* contributions of the wing onto the reflected field could not be exactly the same, which might explain the differences.

Despite these few discrepancies, one can state that the present results comparison is globally very satisfactory, which validates the coupling methodology/functionality and legitimates a posteriori its use for facilitating such an installed engine noise assessment through a structured full-CAA approach.

Once this validation step had been achieved through the solving of the no-flight configuration, its in-flight counterpart was conducted.

E. Mean-Flows Interpolation

No full-3D RANS simulation having been computed over the complete exhaust + airfoil installed configuration, the sole available mean-flow material came from two separate (2D-axi and 2D) RANS calculations, which were originally conducted over each one of the two solid bodies, this having been done using ONERA's *elsA* CFD solver.[¶] It was then necessary to merge these two distinct isolated configuration RANS results into a single installed configuration CAA background mean flow, which was a tricky operation for two reasons. First, from a physical point of view, the resulting merged mean flow was to be as close as possible to the two distinct initial ones, a requirement that led to developing an original matching approach (see below). Second, from a more practical point of view, the CFD → CAA interpolation of this merged mean-flow RANS material required numerous successive grid and mean-flow manipulations (crossed CFD/CFD interpolations, CFD/CAA remeshing and interpolation processes, etc.).

To match such exhaust and airfoil RANS mean flows, two successive operations were needed. First, the airfoil mean flow was scaled in order that its quantities at infinity (superscript "∞") fit well with that of the exhaust's mean flow. This was done considering the appropriate conservation law for both the ratio v_o/v_o^∞ and the ratio $(p_o - p_o^\infty)/q_o^\infty$ (where p_o, v_o, and q_o stand, respectively, for the aerodynamic local pressure, velocity, and kinetic energy). Secondly, the effective merging was conducted with the help of a simple algebraic manipulation of the conservative variables ($U_o^{\text{merged}} = U_o^{\text{exhaust}} + U_o^{\text{airfoil}} - U_o^\infty$), so that both the exhaust and the airfoil vicinities recover naturally their own initial mean-flow patterns.

Once this merged RANS mean-flow material was available, it was interpolated over the two (exhaust and airfoil) CAA body-fitted grids, thanks to the bilinear interpolation feature of a commercial graphic solver. Concerning the background Cartesian grid, such a CFD → CAA interpolation task was not as straightforward at all. In particular, it required numerous preliminary manipulations in order to obtain a well-defined mean flow over the ex-hole zones (exhaust and airfoil interior areas).

As can be seen on Fig. 8, the final result of all these merging/interpolating processes is very satisfactory, providing a perfectly continuous background mean flow.

At this stage, it has nevertheless to be said that uncertainty remains regarding the overall validity of this matched mean-flow approach, which, once again, was driven by the fact that the only available RANS material came from two separate 2D and 2D-axi CFD computations, instead of one single full-3D calculation. Actually,

[¶]Data available online at http://elsa.onera.fr/

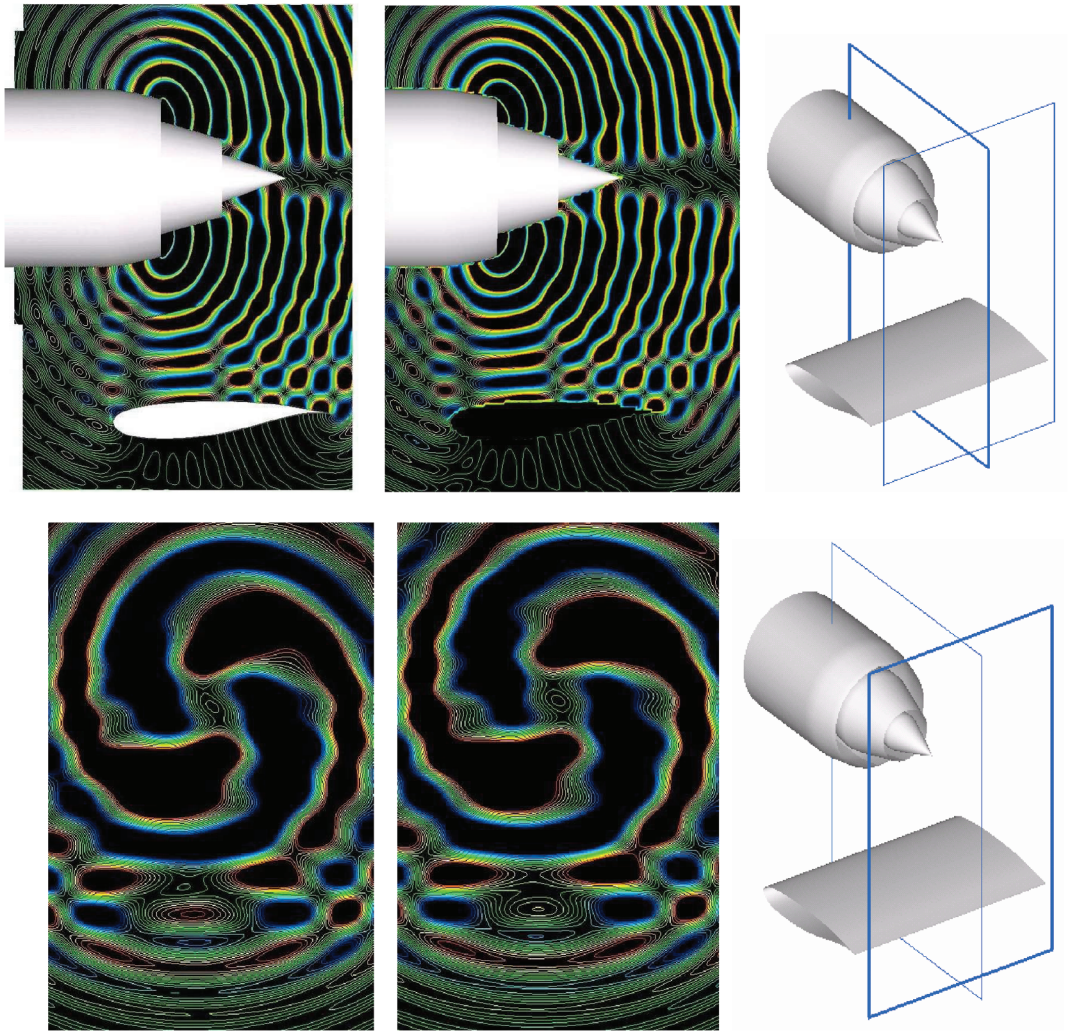

Fig. 6 Aft fan noise radiation of the installed engine in static conditions (medium at rest). sAbrinA (left) and ACTI3S (center) calculations: instantaneous perturbed pressure fields obtained at the end of the simulation, plotted over two lateral planes (sketched in blue on the right sides of the figure).

independently of how correct the CAA computations are, the relevance of the final results should be very dependent on how this merged mean flow is close to the one that a real installed configuration RANS computation would have provided. This question will remain open until such a 3D calculation is conducted over the whole exhaust + airfoil configuration.

F. Aft Fan Noise Radiation of the Installed Engine Considered Under a Takeoff Flight Condition

Because of the higher CFL constraints inherited from the mean-flow field strong heterogeneities, the time step had to be reduced to a value corresponding to one 325th of the acoustical source period (T). Apart from this point, the computational setup of the present in-flight simulation was similar to the previous one.

Figure 9 displays two plots of the instantaneous perturbed pressure field obtained at the end of the simulation. Here too, from a pure numerical point of view, one can firstly appreciate the perfect continuity of the perturbed field at the crossing of the two curvilinear/Cartesian grids interfaces, as well as the robustness of the exit boundary condition imposed at the Cartesian domain periphery. One can also notice that the emitted acoustic waves are not polluted by any hydrodynamic instability, although they were propagated over a background mean flow of quite severe characteristics (in terms of velocity/density/pressure gradients, and of maximum Mach number 0.9). At this stage, it can be underlined that for such calculation, full Euler's (perturbed) equations were used without requiring the suppression of any mean-flow gradient terms, as seems to be necessary when linearized Euler equations are used to solve similar problems [27,28].

From a more physical point of view, one can observe that, compared with the medium at rest case previously detailed, the acoustic radiation patterns are here much more directive, being strongly deflected in the radial directions. This deflection is simply due to the refraction effects, which occur whenever an acoustic wave propagates over shear layers of a jet mean flow [3,4,9]. With respect to the acoustic installation effects matter, such a radial deflection is of importance since it strongly affects the natural radiation pattern of the considered fan noise. In particular, in the present case, the emitted waves are reorientated toward the airfoil suction side, which results in a higher efficiency of the shielding feature offered by the profile. At this stage, one can remark that the present engine $\leftrightarrow$ airfoil positioning seems to have been correctly prescribed, since it leads to a very efficient acoustic shielding; more important than for the medium at rest case, acoustic waves are mainly reflected toward the upper part of the domain, i.e., toward the sky region. However, here again, one needs to remember that such results remain (heavily) subject to the particular radiation pattern characterizing the present fan noise emission. For a more precise assessment of the overall airfoil's shielding efficiency, it shall be necessary to conduct new simulations with other aft fan noise modal contents. In the same manner, additional computations shall also have to be performed for

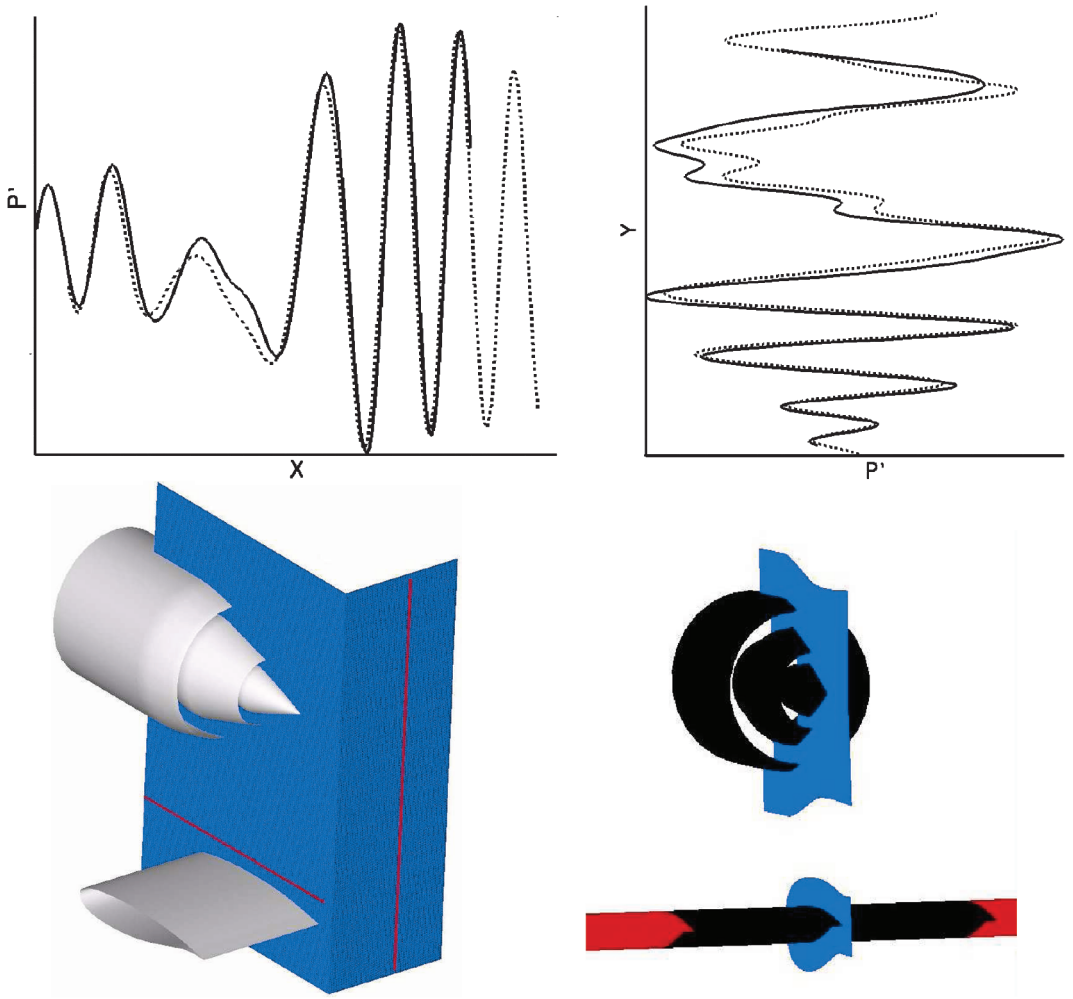

Fig. 7 Aft fan noise radiation of the installed engine in static conditions (medium at rest). sAbrinA (top, bold lines) and ACTI3S (top, dotted lines) calculations: instantaneous perturbed pressure fields obtained at the end of the simulation, plotted over two mesh lines (indicated in red on the left lower part of the figure). Right lower part of the figure: spanwise solid boundary extents for sAbrinA (black) and ACTI3S (red).

background mean flows corresponding to other flight conditions (approach, etc.), for which refraction effects may strongly differ from the present ones. These particular points will be investigated in the near future.

Finally, from a more global/methodological point of view, one can be convinced in light of the present results that structured full-CAA methods seem to be particularly appropriate for solving installed engine noise problems, such methods presenting a maximum of

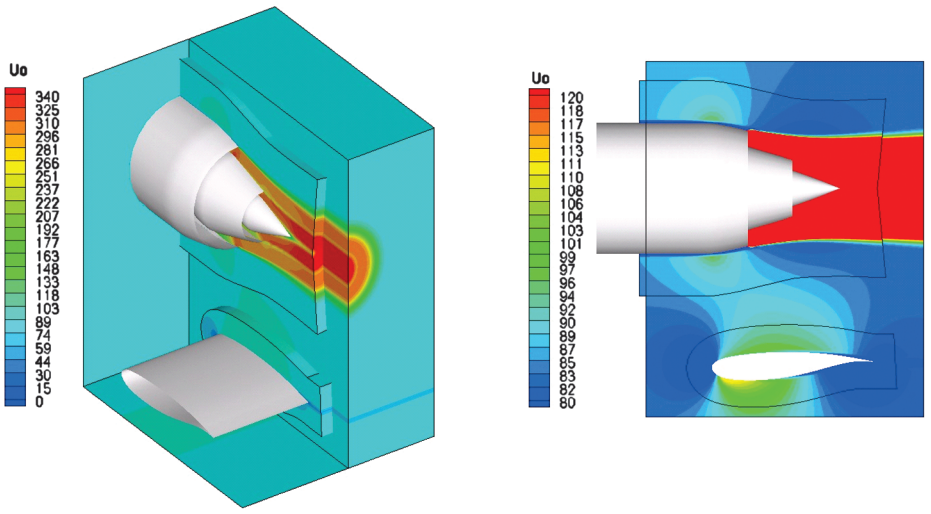

Fig. 8 Aft fan noise radiation of the installed engine in takeoff conditions. elsA calculations: axial velocity field of the merged jet and airfoil mean flows, plotted over both a 3D domain (of half the computational domain, left side) and a lateral plane (right side).

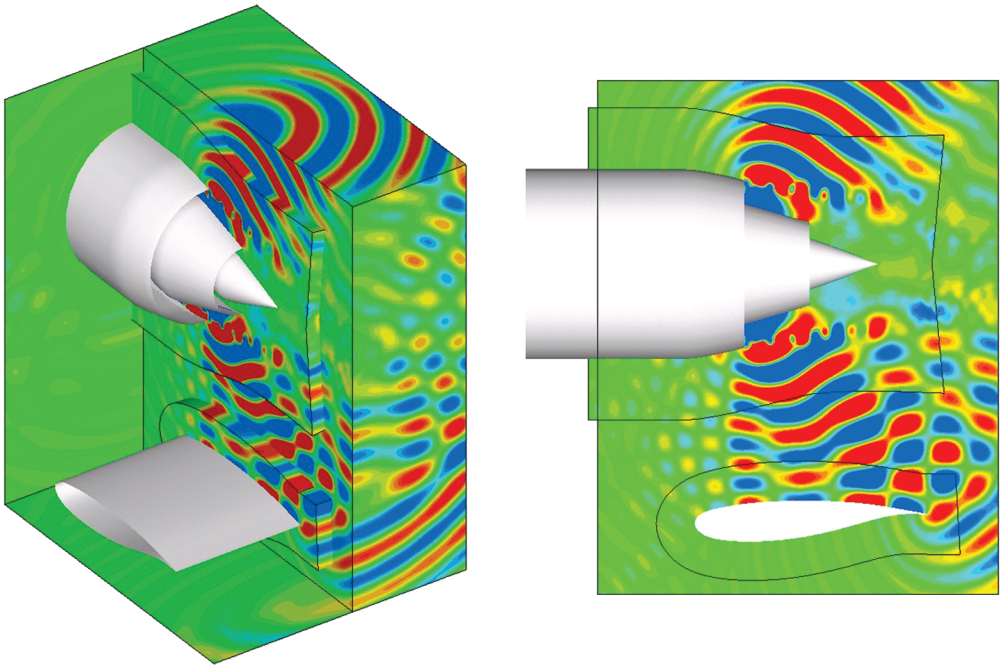

Fig. 9 Aft fan noise radiation of the installed engine in takeoff conditions. sAbrinA calculation: instantaneous perturbed pressure field obtained at the end of the simulation, shown as both a 3D view (of half the computational domain, left side) and a lateral view (right side).

accuracy as well as a minimum of flexibility (especially when used with a coupling approach, as here). Such a conclusion constitutes an important (though indirect) outcome for the present study, and legitimates a posteriori the structured full-CAA strategy adopted for achieving it.

V. Conclusions

In this study related to acoustic installation effects, the engine noise reduction characterizing innovative aircraft configurations was numerically assessed. More precisely, the potential acoustic shield that an empennage airfoil could provide against the aft fan noise of a coaxial engine was numerically predicted, via a structured CAA method/solver. After a description of both the numerical methodology adopted and the pretreatment tasks achieved, several 3D calculations were presented. Involving an engine installed over an empennage wing and considered under both no-flight (medium at rest) and in-flight (takeoff) conditions, such computations deliver various substantial insights of a numerical, physical, methodological, and conceptual nature.

Among the most important outcomes, from a methodological point of view, the study indirectly demonstrated that installed engine noise problems could be assessed as accurately as easily via structured full-CAA approaches. Such methods offering naturally an excellent quality–price ratio (high fidelity versus CPU requirements), they just need a relaxation of their intrinsic meshing constraints, which can be achieved through additional features such as the coupling methodology used and validated here.

From a more conceptual point of view, these calculations have highlighted how RFN configurations could be particularly efficient in terms of aft fan noise reduction, constituting therefore a promising approach for improving aircraft acoustic signatures. The next step of this work will consist in extending the present investigation to other fan noise material (in terms of modal content and/or frequency) and background mean flows (approach flight condition), in order to assess whether such a conclusion can be generalized, and how.

Acknowledgments

The authors acknowledge both Airbus acoustic and aerodynamic teams, which have actively contributed to the test case definition and part of the RANS computations, respectively. In particular, the authors are grateful to Julien Ricouard and to Bastien Caruelle, who indirectly contributed to the complete achievement of the study.

References

[1] Manoha, E., Juvigny, X., and Roux, F. X., "Numerical Simulation of Aircraft Engine Installation Acoustic Effects," *11th AIAA/CEAS Aeroacoustics Conference*, AIAA Paper No. 2005-2920, Monterey, CA, 23–25 May 2005.

[2] Redonnet, S., Parzani, C., Manoha, E., and Lizarazu, D., "Numerical Study of 3D Acoustic Installation Effects through a Hybrid Euler/BEM method," *13th AIAA/CEAS Aeroacoustics Conference*, AIAA Paper No. 2007-3500, Roma, Italy, May 2007.

[3] Polacsek, C., Burguburu, S., Redonnet, S., and Terracol, M., "Numerical Simulations of Fan Interaction Noise using a Hybrid Approach," *AIAA Journal*, Vol. 44, No. 6, 2006, pp. 1188–1196.

[4] Redonnet, S., Manoha, E., and Kenning, O., "Numerical Simulation of the Downstream Fan Noise and Jet Noise of a Coaxial Jet with a Shielding Surface," *10th AIAA/CEAS Aeroacoustics Conference*, AIAA Paper No. 2004-2991, Manchester, England, U.K., 10–12 May 2004.

[5] Redonnet, S., Manoha, E., and Kenning, O., "Numerical Simulation of the Downstream Fan Noise of 3D Coaxial Engines," *11th AIAA/CEAS Aeroacoustics Conference*, AIAA Paper No. 2005-2816, Monterey, CA, 23–25 May 2005.

[6] Redonnet, S., Manoha, E., and Sagaut, P., "Numerical Simulation of Propagation of Small Perturbations Interacting with Flows and Solid Bodies," *7th CEAS/AIAA Aeroacoustics Conference*, AIAA Paper No. 2001-2223, Maastricht, The Netherlands, 28–30 May 2001.

[7] Redonnet, S., "Simulation de la Propagation Acoustique en Présence d'Écoulements Quelconques et de Structures Solides, par Résolution Numérique des Équations d'Euler," Ph.D. Thesis, Université Bordeaux I, Bordeaux, France, Nov. 2001.

[8] Manoha, E., Herrero, C., Sagaut, P., and Redonnet, S., "Numerical Prediction of Airfoil Aerodynamic Noise," *8th CEAS/AIAA Aeroacoustics Conference*, AIAA Paper No. 2002-2573, Breckenridge, CO, 17–19 June 2002.

[9] Terracol, M., Manoha, E., Herrero, C., Labourasse, E., Redonnet, E. S., and Sagaut, P., "Hybrid Methods for Airframe Noise Numerical Prediction," *Theoretical and Computational Fluid Dynamics*, Vol. 19, No. 3, 2005, pp. 197–227.

[10] Dunn, M. H., and Tinetti, A. F., "Aeroacoustic Scattering via the Equivalent Source Method," *10th AIAA/CEAS Aeroacoustics Conference*, AIAA Paper No. 2004-2937, Manchester, England, U.K., May 2004.

[11] Posey, W., Tinetti, A. F., and Dunn, M. H., "The Low-Noise Potential of

Distributed Propulsion on a Catamaran Aircraft," *11th AIAA/CEAS Aeroacoustics Conference*, AIAA Paper No. 2006-2622, Cambridge, MA, May 2006.

[12] Tinetti, A. F., and Dunn, M. H., "Scattering of High Frequency Duct Noise by Full Scale Hybrid Wing Body Configurations," *14th AIAA/CEAS Aeroacoustics Conference*, AIAA Paper No. 2009-3400, Miami, FL, May 2009.

[13] Redonnet, S., Mincu, C., and Manoha, E., "Computational Aeroacoustics of Realistic Co-Axial Engines," *14th AIAA/CEAS Aeroacoustics Conference*, AIAA Paper No. 2008-2826, Vancouver, BC, Canada, May 2008.

[14] Redonnet, S., Mincu, C., Manoha, E., Sengissen, A., and Caruelle, B., "Computational Aeroacoustics of a Realistic Co-Axial Engine in Subsonic and Supersonic Take-Off Conditions," *15th AIAA/CEAS Aeroacoustics Conference*, AIAA Paper No. 2009-3240, Miami, FL, May 2009.

[15] Stanescu, D., Xu, J., Hussaini, M. Y., Farassat, F., "Computation of Engine Noise Propagation and Scattering off an Aircraft," *International Journal of Aeroacoustics*, Vol. 1, No. 4, 2002, pp. 403–420. doi:10.1260/147547202765275989

[16] Stanescu, D., Hussaini, M. Y., and Farassat, F., "Aircraft Engine Noise Scattering by Fuselage and Wings: A Computational Approach," *Journal of Sound and Vibration*, Vol. 263, No. 2, 2003, pp. 319–333. doi:10.1016/S0022-460X(02)01126-4

[17] Desquesnes, G., Terracol, M., Manoha, E., and Sagaut, P., "On the Use of a High-Order Overlapping Grid Method for Coupling in CFD/CAA," *Journal of Computational Physics*, Vol. 220, No. 1, 2006, pp. 355–382. doi:10.1016/j.jcp.2006.05.019

[18] Desquesnes, G., "Couplage par Recouvrement de Maillages Curviligne/Cartésien pour la Simulation Numérique en Aéroacoustique," Ph.D. Thesis, Paris VI University, Paris, France, 2007.

[19] Redonnet, S., Desquesnes, G., Manoha, E., and Terracol, M., "Numerical Study of Acoustic Installation Effects onto the Aft Fan Noise of a Coaxial Engine," *9th Western Pacific Acoustics Conference*, WESPAC Paper 117, Seoul, Korea, 2006.

[20] Poinsot, T. J., and Lele, S. K., "Boundary Conditions for Direct Simulations of Viscous Compressible Flows," *Journal of Computational Physics*, Vol. 101, No. 1, 1992, pp. 104–129. doi:10.1016/0021-9991(92)90046-2

[21] Thomson, K. W., "Time-Dependent Boundary Conditions for Hyperbolic Systems," *Journal of Computational Physics*, Vol. 68, No. 1, 1987, pp. 1–24. doi:10.1016/0021-9991(87)90041-6

[22] Delfs, J. W., "An Overlapped Grid Technique for High Resolution CAA Schemes for Complex Geometries," AIAA Paper 2001-2199, May 2001.

[23] Sherer, S. E., and Scott, J. N., "Development and Validation of a High-Order Overset Grid Flow Solver," *32th AIAA Fluid Dynamics Conference and Exhibit*, AIAA Paper No. 2002-2733, St Louis, MO, June 2002.

[24] Lee, Y., and Baeder, J. D., "High-Order Overset Method for Blade Vortex Interaction," *40th AIAA Aerospace Sciences Meeting*, AIAA Paper No. 2002-0559, Reno, NV, Jan. 2002.

[25] Steger, J. L., Dougherty, F. C., and Benek, J. A., "A Chimera Grid Scheme," *Advances in Grid Generation*, Vol. 5, The American Society of Mechanical Engineers, Fairfield, NJ, 1983, pp. 59–69.

[26] Denelvo, A., Le Saint, S., Sylvand, G., and Terrasse, I., "Numerical Methods: Fast Multipole Method for Shielding Effects Noise of a Coaxial Engine," *11th AIAA/CEAS Aeroacoustics Conference*, AIAA Paper No. 2005-2971, Monterey, CA, May 2005.

[27] Zhang, X., Chen, X. X., Morfey, C. L., and Tester, B. J., "Computation of Fan Noise Radiated through a Realistic Engine Exhaust Geometry with Flow," *9th AIAA/CEAS Aeroacoustics Conference*, AIAA Paper 2003-3282, Hilton Head, SC, 12–14 May 2003.

[28] Tester, B. J., and Gabard, G., "Influence of Mean Flow Gradients on Fan Exhaust Noise Prediction," *14th AIAA/CEAS Aeroacoustics Conference*, AIAA Paper No. 2008-2825, Vancouver, BC, Canada, May 2008.

J. Astley
Associate Editor